DOI: 10.17516/1997-1397-2022-15-6-687-698
УДК 535.42

The Talbot Effect under Selective Reflection from a Raman Induced Grating

Vasily G. Arkhipkin*
Sergey A. Myslivets†
Kirensky Institute of Physics
Federal Research Center KSC SB RAS
Krasnoyarsk, Russian Federation
Siberian Federal University
Krasnoyarsk, Russian Federation

Received 10.05.2022, received in revised form 18.07.2022, accepted 20.09.2022

Abstract. In the present work, we study the Talbot effect under selective reflection of probe radiation at the interface between a dielectric and a layer of resonant atoms, in which a Raman grating is induced. Under such conditions, the interface can operate as a reflective diffraction grating. The cases of one- and two-dimensional gratings are considered. It is shown that the reflection coefficient, with the account of the selectively reflected wave, can be both greater or smaller than the usual Fresnel reflection coefficient. The Talbot effect can be observed for a selectively reflected wave in the near-field diffraction region. The spatial structure of the diffraction patterns essentially depends on the pump field intensity and the Raman detuning.

Keywords: Raman gain, Fresnel diffraction, Talbot effect, selective reflection.

Citation: V.G. Arkhipkin, S.A. Myslivets, The Talbot Effect under Selective Reflection from a Raman Induced Grating, J. Sib. Fed. Univ. Math. Phys., 2022, 15(6), 687–698.
DOI: 10.17516/1997-1397-2022-15-6-687-698.

Introduction

When a plane monochromatic light wave propagates through a periodic grating (structure), the Talbot effect (ET) can be observed, which involves periodic self-reproducing of the grating image at distances a multiple of the Talbot length [1, 2]. This phenomenon is a consequence of interference between diffraction orders in the near field (Fresnel diffraction) and takes place for waves of any nature. This effect has been demonstrated on atomic waves and a Bose-Einstein condensate [3], surface plasmon polaritons [4], exciton polaritons [5], in metamaterials [6], etc. Recently, it was observed on gratings based on electromagnetically induced transparency [7,8]. A possibility of observing ET with amplification [9] on an induced Raman grating [10,11] was shown. The ET has extensive applications in various fields [2]: interferometry [12], optical imaging and computing [13], optical microscopy [14], lithography [15], etc. It is a powerful tool to study the properties of surfaces, particularly to measure the quality of reflective gratings [16, 17] and surface microstructuring [18]. In [19], the ET was considered in the case of selective reflection of light from a homogeneous atomic medium under electromagnetically induced transparency. Reflection of radiation from the interface between a dielectric and an atomic medium is called a selective reflection (SR) because a spectral structure appears in the reflection spectrum at the frequencies of atomic transitions [20, 21]. The SR is an effective tool for spectral studies of the

*avg@iph.krasn.ru https://orcid.org/0000-0002-7401-2341
†sam@iph.krasn.ru https://orcid.org/0000-0003-2604-2471
© Siberian Federal University. All rights reserved

resonant properties of the medium in the vicinity of the interface with high resolution [22–25]. Based on the SR, a tunable filter [26] and a non-linear beam splitter [27] have been implemented. This method may be of interest for detecting isotopes in natural atomic vapors [28].

In this paper, we study the Talbot effect under selective reflection of probe radiation at the interface between a dielectric and a layer of three-level atoms, in which a Raman grating directed parallel to the interface is induced due to interaction of the probe field with a standing pump wave. The features of ET under these conditions are discussed for various detunings and intensities of the pump field. Upon changing these parameters, the Talbot images for selectively reflected radiation are modified.

1. Theoretical model

Let us consider a homogeneous layer of three-level atoms 2, contained between two transparent dielectrics 1 and 3 (Fig. 1a), located in the regions $z < 0$ and $z > L$, where L is the thickness of the atomic layer. We will assume that the inner surface of the dielectric 3 has an anti-reflection coating, so the reflection from this interface can be neglected. Fig. 1b shows the energy states of a three-level lambda system with two metastable states $|0\rangle$ and $|2\rangle$, where the frequencies of allowed transitions $|0\rangle$–$|1\rangle$ and $|2\rangle$–$|1\rangle$ are ω_{10} and ω_{12}, respectively. The initially populated state is the ground state $|0\rangle$. A probe monochromatic wave with frequency ω_2 propagates normally to the $1-2$ interface and interacts with a standing pump wave $E_1(x) = E_1 \sin(\pi x/\Lambda)$ with frequency ω_1 (Fig. 1b), directed parallel to the $1-2$ interface (along the x-axis). This wave is produced by two plane waves with the same frequency ω_1, incident at an angle θ to the interface $1-2$ symmetrically to the z-axis. It is them that generate a standing wave along the interface in the area of intersection with a spatial period of $\Lambda = \lambda_1/2\sin\theta$ where λ_1 is the wavelength of the pump field E_1.

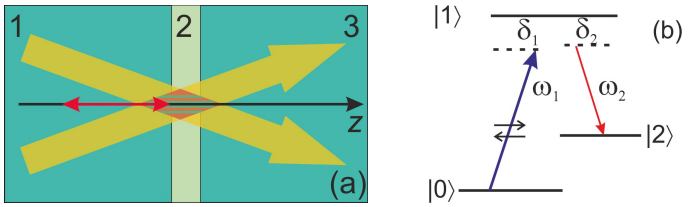

Fig. 1. a) The geometry of the probe field (red arrow) and pump fields (thick yellow arrows) incident on homogeneous gas of atoms confined between two dielectrics 1 and 3. The red arrow in the opposite direction is the reflected probe field. b) The energy states of three-level lambda-type atoms: ω_1 is the frequency of the standing pump wave interacting with the transition $|0\rangle - |1\rangle$, ω_2 is the frequency of the probe field (Raman field) interacting with the transition $|2\rangle - |1\rangle$

The probe monochromatic wave E_{2i} incident on the interface $1-2$ is partially reflected (E_{2r}) and partially propagates through the atomic medium (E_{2t}). The electric field of these waves can be written in the form

$$\begin{aligned} E_{2i} &= E_0 \exp[-i(\omega_2 t - k_2 n_1 z)], \\ E_{2r} &= E_R \exp[-i(\omega_2 t + k_2 n_1 z)], \\ E_{2t} &= E_T \exp[-i(\omega_2 t - k_2 n_3 z + \phi)], \end{aligned} \tag{1}$$

where $k_2 = \omega_2/c$, $\varphi = k_2 L(n_3 - n_2)$, n_i $(i = 1, 2, 3)$ are the refractive indices of the corresponding medium. The probe wave field with frequency ω_2 in an atomic medium E_{2m} can be represented as $E_{2m} = \mathcal{E}_2(z)\exp[-i(\omega_2 t - k_2 z)] = E_2(z)\exp(-i\omega_2 t)$. Here $\mathcal{E}_2(z)$ is the probe field amplitude

in the atomic medium. The continuity condition for these fields and their derivatives at the interfaces $z = 0$ and $z = L$ has the form:

$$\begin{aligned} E_2(z=0) &= E_0 + E_R \\ \partial E_2(z)/\partial z\,|_{z=0} &= in_1k_2(E_0 - E_R) \\ E_2(z=L) &= E_T \exp(ik_2L) \\ \partial E_2(z)/\partial z\,|_{z=L} &= in_3k_2E_T \exp(ik_2L). \end{aligned} \tag{2}$$

From boundary conditions (2), it is possible to find the amplitude reflection coefficient of the probe wave $r = E_R/E_0$ as

$$r = \frac{ik_2n_1E_2(0) - \partial E_2(z)/\partial z\,|_{z=0}}{ik_2n_1E_2(0) + \partial E_2(z)/\partial z\,|_{z=0}}. \tag{3}$$

Note that the expression (3) takes into account both nonresonant (Fresnel) and resonant (selective) reflection. In our opinion, such a parameter is more convenient in the experiment, since it is rather problematic in practice to identify the resonant reflection against the Fresnel background.

First, consider the case of a one-dimensional (1D) standing pump wave along the interface: $E_1(x) = E_1 \sin(\pi x/\Lambda)$. The propagation of the probe field in the Raman system is described by wave equations. In the given pump field approximation and a slowly varying probe field amplitude $|\partial^2\mathcal{E}_2/\partial z^2| \ll k_2|\partial\mathcal{E}_2/\partial z|$, equation for the amplitude $\mathcal{E}_2$ becomes (see, for example [29])

$$\frac{\partial^2\mathcal{E}_2}{\partial x^2} + 2ik_2\frac{\partial\mathcal{E}_2}{\partial z} = -4\pi k_2^2\chi_R\mathcal{E}_2, \tag{4}$$

where χ_R is the Raman susceptibility of an atomic medium for a probe wave in the presence of a pump field, and it has the form [30]:

$$\chi_R = \alpha_r\frac{\gamma_{12}|G_1|^2\sin^2(\pi x/\Lambda)}{\delta_1^2[(\delta_{20} + i\gamma_{20}) + (|G_1|^2/\delta_1)\sin^2(\pi x/\Lambda)]}, \qquad \alpha_r = \frac{|d_{12}|^2N}{2\hbar\gamma_{12}}, \tag{5}$$

where $\delta_1 = \omega_1 - \omega_{10}$, $\delta_2 = \omega_2 - \omega_{12}$ are the one-photon detunings, $\delta_{20} = \omega_1 - \omega_2 - \omega_{20}$ is the Raman (two-photon) detuning, ω_{mn}, γ_{mn}, d_{mn} are the frequency, half-width and dipole matrix element of the respective transitions, N is the density of atoms, $\hbar$ is the reduced Planck's constant. $G_1 = d_{10}E_1/2$ is the Rabi frequency, E_1 is the amplitude of the standing pump wave. Formula (5) is written assuming $\delta_1 \approx \delta_2$.

Expression (5) shows that the susceptibility χ_R is periodically spatially modulated with a standing wave period Λ in the x-direction perpendicular to the propagation direction z. Thus, when the pump field is a standing wave, the Raman amplification and dispersion of the probe field can become spatially periodic, and the atomic medium acts like a grating, which is referred to as Raman induced grating (RIG) [30]. It can be seen from(5) that for the Stark shift $S = |G_1|^2/|\delta_1| \gg \gamma_{20}$ (a strong pump field), the resonance frequency of the Raman transition is shifted. In contrast, for $S \ll \gamma_{20}$ (a weak pump field), the susceptibility coincides with that in the perturbation theory approximation [31]. Fig. 2 shows $\mathrm{Im}\,\chi_R$ and $\mathrm{Re}\,\chi_R$ as a function of the Raman detuning δ_{20} and the transverse coordinate x for a fixed Rabi frequency of the pump field G_1. Parameter values used for calculations are given in Section 2. Negative $\mathrm{Im}\,\chi_R$ means the Raman amplification of the probe field. The $\mathrm{Im}\,\chi_R$ peaks correspond to the Raman resonance adjusted for the Stark shift. The black dashed-dotted curves (Fig. 2b,d) correspond to the case when the Raman resonance occurs for the pump field at the antinode center, and the blue dashed curves refer to the fields on the slopes of the antinode. In this case, one can speak of a spatial splitting of the imaginary part of the Raman susceptibility. The solid pink curve corresponds to the case when the initial Raman detuning is such that, for a fixed pump field, the smallest detuning takes place at the antinode center. It increases on the slopes, which leads to a

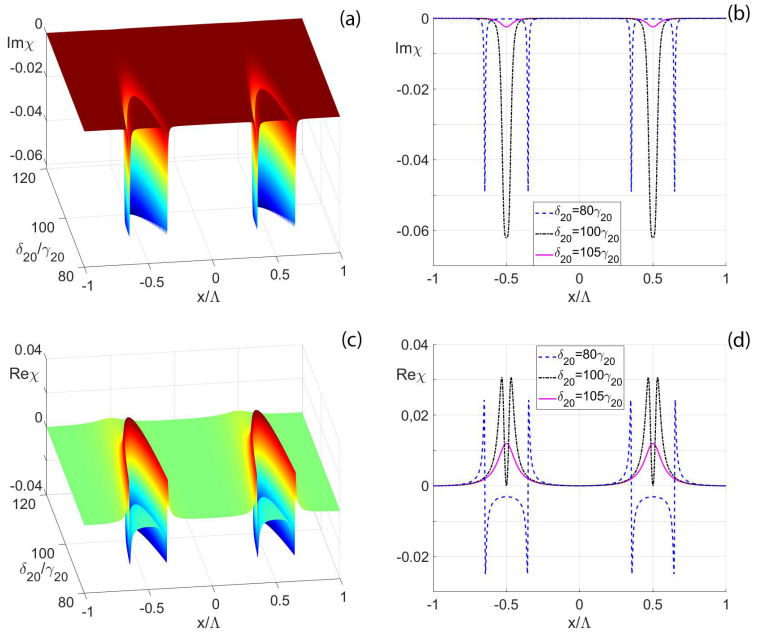

Fig. 2. The dependence of $\mathrm{Im}\,\chi_R$ (a, b) and $\mathrm{Re}\,\chi_R$ (c, d) as a function of the scaled Raman detuning δ_{20} and scaled transverse coordinate x at $G_1 = 10$

decrease in $\mathrm{Im}\,\chi_R$. A similar behavior of it is observed for a fixed Raman detuning and various pump fields.

Assuming that the probe wave is plane and the Fresnel number is $N_F = \Lambda^2/4\lambda_2 L \gg 1$ (diffraction-free approximation), the solution of the (4) equation for the field $E_2 = \mathcal{E}_2 \exp(ik_2 z)$ in an atomic medium can be written as [32]:

$$E_2(z) = E_2(0) \exp\left[ik_2(1 + 2\pi\chi_R)z\right], \tag{6}$$

where $0 \leqslant z \leqslant L$. Note that the diffraction-free approximation $N_F \gg 1$ imposes a limitation on the atomic layer thickness L.

Using expression (6), the reflection coefficient (3) acquires the form:

$$r = \frac{n_1 - (1 + 2\pi\chi_R)}{n_1 + (1 + 2\pi\chi_R)} = r_F \frac{1 - 2\pi\chi_R/(n_1 - 1)}{1 + 2\pi\chi_R/(n_1 + 1)}, \tag{7}$$

where $r_F = (n_1 - 1)/(n_1 + 1)$ is the conventional Fresnel reflection coefficient at the $1-2$ interface.

Note that, in contrast to [19], where only selective reflection is analyzed, the reflection coefficient (7) was written taking into account Fresnel and selective reflection. We can say that the Fresnel reflection coefficient is modulated by selective reflection. Expression (7) shows that the reflection coefficient is a periodic function of x with a period of Λ. Therefore, such a structure at the interface operates like a reflective grating, and the probe field incident thereon can be diffracted upon reflection.

In the Fresnel approximation (the near diffraction field), the reflected probe field in the observation plane $E_2(X, Z)$ can be calculated using the Kirchhoff-Fresnel integral [33]

$$E_2(X, Z) = \frac{1 + i}{\sqrt{2\lambda_2 Z}} \exp\left(in_1 k_2 Z\right) E_2(0) \int_{-\infty}^{\infty} r(x) \exp\left[\frac{in_1 k_2}{2Z}(x - X)^2\right] dx, \tag{8}$$

where X and Z are coordinates in the observation plane. Expanding $r(x)$ into a Fourier series and integrating (8), the field $E_2(X, Z)$ can be represented as

$$E_2(X, Z) = E_2(0) \exp(in_1 k_2 Z) \sum\nolimits_m C_m \exp(i2\pi mX/\Lambda - i2\pi m^2 Z/Z_T). \quad (9)$$

Here $Z_T = 2n_1\Lambda^2/\lambda_2$ is the Talbot length, C_m are the Fourier coefficients of the function $r(x)$

Equation (9) contains all the typical features of ET. In particular, for $Z_n = nZ_T$ (n is a positive integer), distribution of the field $E_2(Z_n)$ coincides with the field at the interface $E_2(z = 0)$, i.e. in these planes, the reflected field is an image of the field at the interface. In the case of fractional ET, at distances $Z = (p/q)Z_T$ (p and q are positive integers, $p < q$), the field distribution over X also has a periodic character, but its spatial structure may differ significantly from that at the interface.

The above situation is based on a one-dimensional RIG in an atomic medium. A two-dimensional RIG can be produced using a similar method. In this case, the pump field is generated by two standing waves with the same frequency, directed perpendicular to each other along the x and y axes

$$E_1(x, y) = E_1 \left[\sin(\pi x/\Lambda_x) + \sin(\pi y/\Lambda_y)\right].$$

Further, we will assume that the periods of standing waves along the transverse axes are the same: $\Lambda_x = \Lambda_y = \Lambda$. The expression for the Raman susceptibility takes the form

$$\chi_R = \alpha_r \frac{\gamma_{12}}{\delta_1^2} \frac{|G_1|^2 \left[\sin(\pi x/\Lambda) + \sin(\pi y/\Lambda)\right]^2}{\delta_{20} + i\gamma_{20} + (|G_1|^2/\delta_1)\left[\sin(\pi x/\Lambda) + \sin(\pi y/\Lambda)\right]^2}. \quad (10)$$

The field in the atomic layer and the reflection coefficient are also determined by formulas (6) and (7), respectively, however here χ_R is determined by expression (10). From (7), with the account of (10), it can be seen that the Raman susceptibility and reflection coefficient are 2D periodic functions along the x and y directions with the period $\Lambda_1 = 2\Lambda$. Fig. 3 shows typical dependences of $\mathrm{Im}\,\chi_R$ on the transverse coordinates x and y for various Raman detunings δ_{20} and a fixed value of G_1, which have the form of periodic columnar structures. The dashed-dotted red curve in Fig. 3d corresponds to the perturbed Raman resonance $\delta_{20} + |G_1|^2/\delta_1 = 0$ (when $\sin(\pi x/\Lambda) + \sin(\pi/\Lambda) = 2$). Detuning from the perturbed resonance gives rise to a cavity inside a column, and the transverse size of the column increases (Fig. 3d). Similar dependences are also observed for different values of G_1 and a fixed value of δ_{20}.

For a 2D grating, the reflected probe field $E_2(X, Y, Z)$ at a distance of Z from the interface is defined as:

$$E_2(X, Y, Z) = \frac{i}{\lambda_2 Z} e^{in_1 k_2 Z} E_2(0) \iint_{-\infty}^{\infty} r(x, y) \exp\left\{\frac{in_1 k_2}{2Z}\left[(x - X)^2 + (y - Y)^2\right]\right\} dxdy. \quad (11)$$

Expanding $r(x, y)$ into a double Fourier series, the field E_2 can be represented as [9]

$$E_2(X, Y, Z) = e^{in_1 k_2 Z} \sum_{n,m} C_{n,m} \exp(i2\pi nX/\Lambda_1 + i2\pi mY/\Lambda_1) \exp\left[-i\pi\lambda_2 Z(n^2 + m^2)/n_1\Lambda_1^2\right], \quad (12)$$

where $C_{n,m}$ are the Fourier coefficients of the function $r(x, y)$.

From (12), it can be seen that, like in the case of a 1D grating, the Talbot length for a 2D grating with the same periods along the x and y-axes is $Z_T = 2n_1\Lambda_1^2/\lambda_2$. At a distance of Z_T, all diffraction orders are in phase, and the diffraction pattern is an image of the distribution of the probe field at the interface.

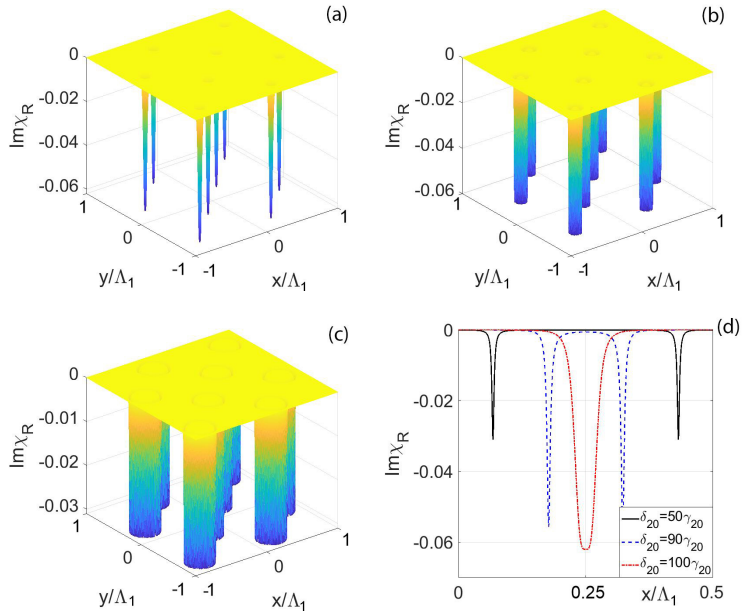

Fig. 3. The dependence $\mathrm{Im}\,\chi_R$ as a function of transverse coordinates x and y at $\delta_{20} = 100$ (a), $\delta_{20} = 90$ (b), $\delta_{20} = 50$ (c), $G_1 = 5$. (d) – The $\mathrm{Im}\,\chi_R$ profile along the x axis ($y = 0.25\Lambda_1$) for various Raman detunings δ_{20}

2. Results and discussion

In the numerical analysis, we used the parameters corresponding to the D_1 sodium line, where the $|0\rangle$ and $|2\rangle$ levels correspond to metastable hyperfine sublevels of the $^2S_{1/2}$ ground state. The following parameter values were used in the calculations: $\gamma_{10}/2\pi = 10$ MHz, $\gamma_{21} = \gamma_{10}$, $\gamma_{20} = 10^{-3}\gamma_{10}$, $N = 10^{14}$ cm^{-3}. The Rabi frequency G_1 and single-photon detuning δ_1 are given in the units of γ_{10}, the Raman detuning δ_{20} in the units of γ_{20}, $\delta_1 = -100$, and the standing wave period $\Lambda = 200\lambda_1$.

2.1. 1D grating

Fig. 4 shows the behavior of the reflection coefficient for the probe wave $R = |r|^2$ as a function of the transverse coordinate x for various Rabi frequencies of the pump field and Raman detunings. For a fixed Rabi frequency G_1 and varying Raman detuning δ_{20}, the typical behavior of the reflection coefficient is shown in Fig. 4a. The reflection coefficient has a similar form for a fixed Raman detuning and different pump field Rabi frequencies (Fig. 4c). Note that the higher the Rabi frequency of the pump field, the higher maximum values of R are achieved at optimal detunings when a perturbed Raman resonance takes places (Fig. 5). Thus, the probe field distribution along the x-axis at the interface differs from the standing pump wave and has a more complex configuration, which depends on the pump field intensity, the initial Raman detuning and the standing wave period. The latter is determined by the angle θ between the pump fields that generate a standing wave. A change in the angle θ changes the spatial scale of the emerging structures in the field distribution. The resonant structures in the reflection coefficient (Fig. 4b,d) are due to SR from the interface between the dielectric and the layer of three-level atoms with an induced grating since they depend on the Raman detuning. In the region of SR, the reflection coefficient can be both greater or smaller than the Fresnel reflection coefficient,

which under the conditions under consideration corresponds to $R = 0.04$. We emphasize that the reflection coefficient from the interface, considering the SR, is a periodic function along the interface with the period of the standing pump wave Λ.

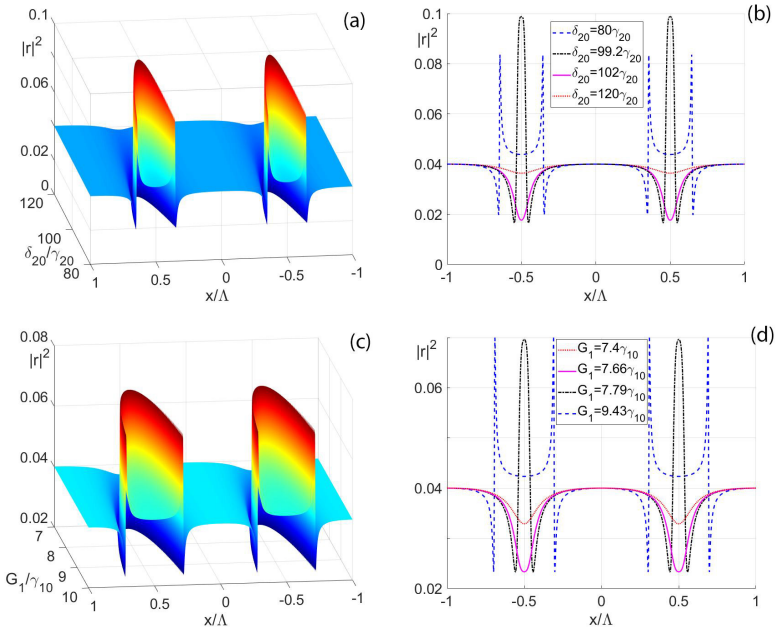

Fig. 4. (a, c) The reflection coefficient $R = |r|^2$ as a function of the normalized transverse coordinate x for various Raman detunings δ_{20} (a) for $G_1 = 10$ and different values of G_1 (c) for $\delta_{20} = 60$. (b, d) The probe field intensity profile at the interface for various Raman detunings δ_{20} (b) for $G_1 = 10$ and different values of G_1 (d) for $\delta_{20} = 60$

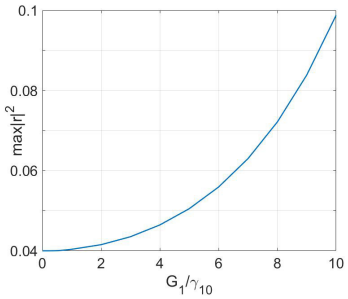

Fig. 5. The dependence of the maximum reflection coefficient $R = |r|^2$ on the normalized Rabi frequency G_1

Fig. 6a,c,e shows diffraction patterns in the near field (the Talbot carpets) of selectively reflected probe radiation and intensity profiles (Fig. 6b,d,f) in different Talbot planes for various Raman detunings and a fixed Rabi frequency of the pump field. At a distance of $Z = Z_T$, the intensity distribution is similar to that at the interface $z = 0$, i.e., it is an image thereof. At the distance $Z = Z_T/2$, the diffraction pattern is also an image of the field distribution at the interface but shifted by half a period. For smaller regular fractions of the Talbot length, periodic structures with period Λ can also be observed. However, within the period, the spatial structure of the pattern differs from the initial distribution of the probe field at the interface (Fig. 6b,d,f,

$Z = Z_T/4$, $Z = Z_T/3$). A similar picture is observed at different Rabi frequencies of the pump field and a fixed Raman detuning. Thus, the spatial structure of diffraction patterns is modified by changing the Raman detuning or the Rabi frequency of the pump field.

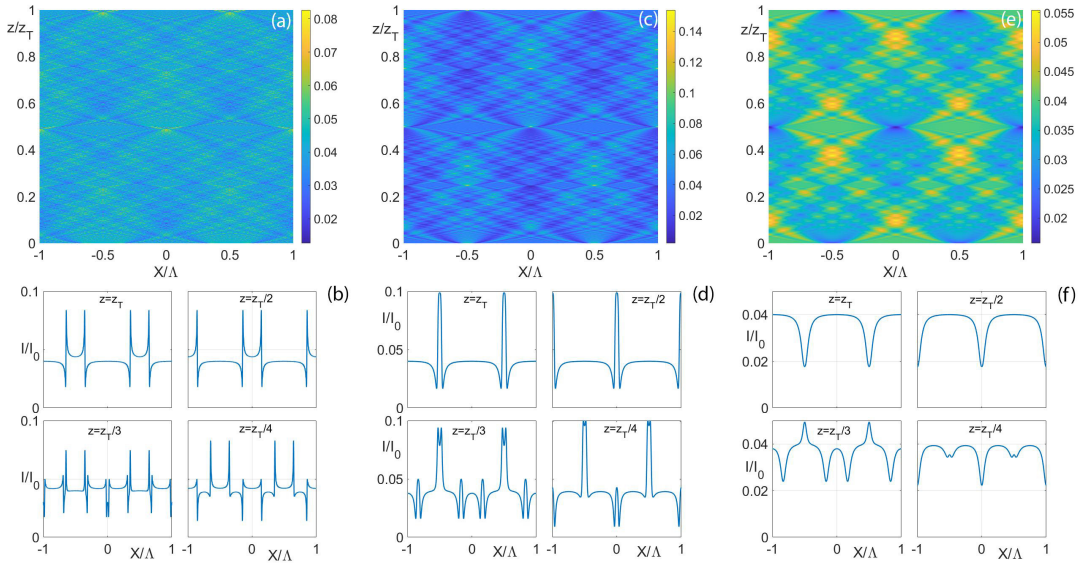

Fig. 6. The Talbot carpet (a, c, e) and the intensity profile in various Talbot planes (b, d, f) at $G_1 = 10$. (a, b) – $\delta_{20} = 80$; (c, d) – $\delta_{20} = 99.2$; (e, f) – $\delta_{20} = 102$

2.2. 2D gratings

In general, the reflection coefficient behavior in a 2D grating is similar to the 1D case, however there are significant differences. First, for a 2D structure, the period in the spatial distribution of the field at the interface changes. This is due to the doubling of the period in the spatial distribution of the Raman susceptibility (see Model section). Fig. 7 shows the behavior of the probe wave reflection coefficient R at the interface as a function of the transverse coordinates for various Raman detunings and a fixed Rabi frequency of the pump field for the case of a 2D grating. It can be seen that reflection coefficient is a 2D periodic function of transverse coordinates with the period $\Lambda_1 = 2\Lambda$. The peaks correspond to the selective reflection that appears near the Raman resonance. In the region of SR, the reflection coefficient depends on the detuning and can be both greater or smaller than the usual Fresnel reflection coefficient. At specific detunings, a dip within the peaks can appear, which can be called a spatial splitting (Fig. 7d). The detunings at which selective reflection occurs depend on the Rabi frequency of the pump field.

The second difference is that for a 2D case, self-imaging of the field distribution at the interface is possible not only at a distance of $Z = Z_T$. This is because, for the chosen configuration of the pump fields creating a standing wave, the Fourier coefficients $C_{n,m}$ in expression (12) are nonzero only if m and n have the same parity [9]. Then, the factor $(n^2 + m^2)$ is always even, and the reflected field distribution in the planes $Z = Z_T$ and $Z = Z_T/2$ coincides with that at the interface. Fig. 8 shows diffraction patterns of selectively reflected probe radiation in different Talbot planes for various Raman detunings and a fixed Rabi frequency of the pump field in the case of a 2D grating. It can be seen that the intensity distribution in the $Z = Z_T$ and $Z = Z_T/2$ planes (Fig. 8a) is similar to the field distribution at the interface ($z = 0$) while in the

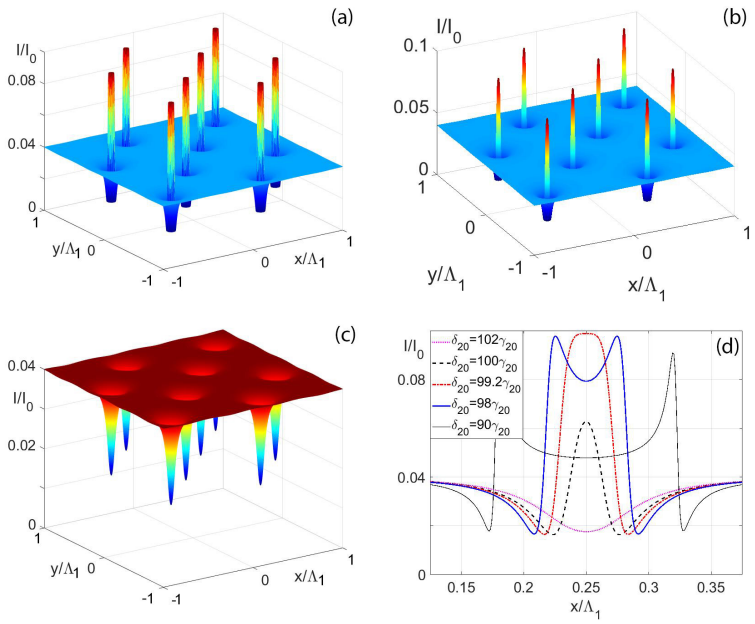

Fig. 7. (a, b, c) The reflection coefficient from the interface as a function of normalized transverse coordinates x and y for various Raman detunins: $\delta_{20} = 98$ (a), $\delta_{20} = 99.2$ (b), $\delta_{20} = 102$ (c), $G_1 = 5$. (d) The single period profile of the probe field intensity at the interface along the x-axis ($y = 0.25\Lambda_1$) for various Raman detunings δ_{20} and $G_1 = 5$

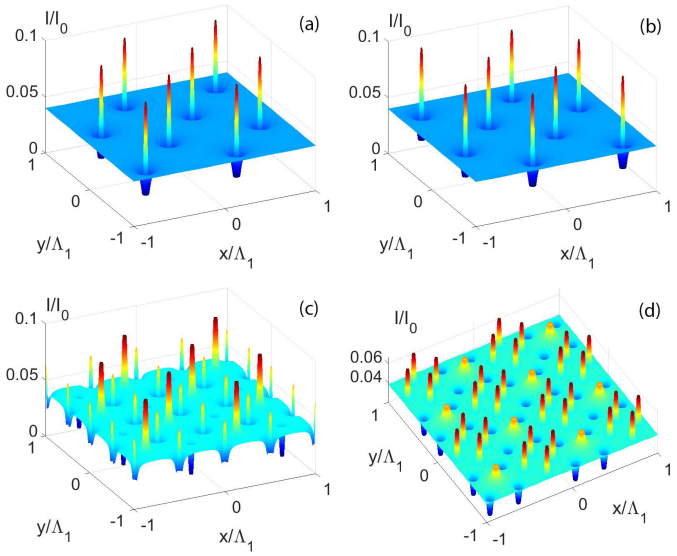

Fig. 8. Normalized intensity of the diffraction patterns in the planes $Z = Z_T$ and $Z = Z_T/2$ (a), $Z = Z_T/4$ (b), $Z = Z_T/8$ (c), $Z = Z_T/3$ (d), $G_1 = 5$

$Z = Z_T/4$ plane (Fig. 8b) it is shifted by half a period. Periodic structures with the period Λ_1 are also observed at other fractions of the Talbot length. However, within the period, the spatial structure of the pattern differs from the initial probe field distribution at the interface and has a more complex spatial geometry. See, for example, Fig. 8c,d, where diffraction patterns are

shown in the $Z = Z_T/8$ and $Z = Z_T/3$ planes, respectively. A similar picture holds for various Rabi frequencies of the pump field and a fixed Raman detuning. Thus, the spatial structure of diffraction patterns is modified by changing the Raman detuning or the Rabi frequency of the pump field.

Conclusion

We have studied the effect of selective reflection of a probe wave at the interface between a dielectric and a layer of atoms, in which a Raman grating is induced along the interface. The cases of one- and two-dimensional gratings have been considered. It is shown that the reflection coefficient adjusted for the selectively reflected wave can be both greater or smaller than the usual Fresnel reflection coefficient. The Talbot effect can be observed for a selectively reflected wave in the near diffraction region. The spatial structure of the diffraction patterns depends on the pump field intensity and the Raman detuning. In the case of a 1D grating, the period of diffraction structures is equal to that of the standing wave. In the Z_T and $Z_T/2$ planes, the diffraction patterns are images of the distribution of the probe field at the interface (the Talbot images), while at $Z_T/2$, the diffraction pattern is shifted by half a period. In the case of a 2D grating, the diffraction patterns period is equal to twice the standing pump wave period; in the Z_T, $Z_T/2$, and $Z_T/4$ planes, the diffraction patterns are images of the field distribution at the interface, while in the $Z_T/4$ plane, the image is shifted by half a period. In the fractional Talbot planes, periodic diffraction patterns are also observed with a period equal to the period of the standing wave in the case of a 1D grating and with twice the period for a 2D grating. However, here the spatial structure of the field becomes more complicated, crucially differing from the distribution of the field at the interface, and depends on the pump field intensity and Raman detuning. The reflection coefficient of a selectively reflected wave can be much higher than in the case of a grating based on electromagnetically induced transparency [19].

This work was partially (results for 1D gratings) supported by the Russian Science Foundation (RSF) through Grant 19-12-00203.

References

[1] K.Patorski, The Self-Imaging Phenomenon and its Applications, In: Progress in Optics, Vol. 27, chap. 1, Elsevier, 1989.

[2] J.Wen, Y.Zhang, M.Xiao, The Talbot effect: recent advances in classical optics, nonlinear optics, and quantum optics, *Adv. Opt. Photon.*, **5**(2013), 83–130. DOI: 10.1364/AOP.5.000083

[3] C.Ryu, M.F.Andersen, A.Vaziri, MB.d'Arcy, J.M.Grossman, K.Helmerson, W.D.Phillips, High-Order Quantum Resonances Observed in a Periodically Kicked Bose-Einstein Condensate, *Phys. Rev. Lett.*, **96**(2006), 160 403. DOI: 10.1103/PhysRevLett.96.160403

[4] W.Zhang, C.Zhao, J.Wang, J.Zhang, An experimental study of the plasmonic Talbot effect, *Opt. Express*, **17**(2009), 19 757–19 762.

[5] T.Gao, E.Estrecho, G.Li, O.A.Egorov, X.Ma, K.Winkler, M.Kamp, C.Schneider, S.Höfling, A.G.Truscott, E.A.Ostrovskaya, Talbot Effect for Exciton Polaritons, *Phys. Rev. Lett.*, **117**(2016), 097 403. DOI: 10.1103/PhysRevLett.117.097403

[6] H.Nikkhah, M.Hasan, T.J.Hall, The Talbot effect in a metamaterial, *Applied Physics A*, **124**(2018), 106. DOI: 10.1007/s00339-017-1521-1

[7] J.Wen, S.Du, H.Chen, M.Xiao, Electromagnetically induced Talbot effect, *Appl. Phys. Lett.*, **98**(2011), 081 108. DOI: 10.1063/1.3559610

[8] J.Yuan, C.Wu, Y.Li, L.Wang, Y.Zhang, L.Xiao, S.Jia,Integer and fractional electromagnetically induced Talbot effects in a ladder-type coherent atomic system, *Opt. Express*, **27**(2019), 92–101.

[9] V.G.Arkhipkin, S.A.Myslivets, Talbot effect based on a Raman-induced grating, *Phys. Rev. A*, **100**(2019), 063 835. DOI: 10.1103/PhysRevA.100.063835

[10] V.G.Arkhipkin, S.A.Myslivets, Raman-induced gratings in atomic media, *Opt. Lett.*, **39**(2014), 3223–3226.

[11] V.G.Arkhipkin, S.A.Myslivets, Coherent manipulation of the Raman-induced gratings in atomic media, *Phys. Rev. A*, **93**(2016), 013 810. DOI: 10.1103/PhysRevA.93.013810

[12] J.C.Bhattacharya, Talbot interferometry in the measurement of the refractive indices of a doubly refracting crystal, *Appl. Opt.*, **40**(2001), 1658–1662 .

[13] J.Garcia-Sucerquia, D.C.Alvarez-Palacio, H.J.Kreuzer, High resolution Talbot self-imaging applied to structural characterization of self-assembled monolayers of microspheres, *Appl. Opt.*, **47**(2008), 4723–4728.

[14] S.Feng, M.Wang, J.Wu, Lensless in-line holographic microscope with Talbot grating illumination, *Opt. Lett.*, **41**(2016), 3157–3160.

[15] Q.Wu, H.Xia, H.Jia, H.Wang, C.Jiang, L.Wang, J.Zhao, R.Tai, S.Xiao, D.Zhang, S.Yang, J.Jiang, Fast and large-area fabrication of plasmonic reflection color filters by achromatic Talbot lithography, *Opt. Lett.*, **44**(2019), 1031–1034.

[16] F.J.Torcal-Milla, L.M.Sanchez-Brea, E.Bernabeu, Talbot effect with rough reflection gratings, *Appl. Opt.*, **46**(2007), 3668–3673.

[17] M.Dashtdar, A.Mohammadzade, S.M.-A.Hosseini-Saber, Measurement of roughness based on the Talbot effect in reflection from rough surfaces, *Appl. Opt.*, **54**(2015), 5210–5215.

[18] M.Aymerich, D.Nieto, M.T.Flores-Arias, Laser-based surface multistructuring using optical elements and the Talbot effect, *Opt. Express*, **23**, 24 369–24 382 (2015).

[19] Y.Li, W.Huang, Talbot effect of selective reflection from a homogeneous atomic vapour, *J. Mod. Opt.*, **64**(2017), 1222–1228. DOI: 10.1080/09500340.2016.1273408

[20] J.Woerdman, M.Schuurmans, Spectral narrowing of selective reflection from sodium vapour, *Opt. Comm.*, **14**(1975), 248–251.

[21] A.M.Akulshin, V.L.Velichanskii, A.S.Zibrov, V.V.Nikitin, V.V.Sautenkov, E.K.Yurkin, N.V.Senkov, Collisional Broadening of Intra-Doppler Resonances of Selective Reflection on the D2 Line of Cesium, *Appl. Phys. Lett.*, **36**(1982), 247–250.

[22] M.Chevrollier, M.Oriá, J.G. de Souza, D.Bloch, M.Fichet, M.Ducloy, Selective reflection spectroscopy of a resonant vapor at the interface with a metallic layer, *Phys. Rev. E*, **63**(2001), 046 610. DOI: 10.1103/PhysRevE.63.046610

[23] A.Laliotis, I.Maurin, M.Fichet, D.Bloch, M.Ducloy, N.Balasanyan, A.Sarkisyan, D.Sarkisyan, Selective reflection spectroscopy at the interface between a calcium fluoride window and Cs vapour, *Applied Physics B*, **90**(2008), 415–420.
DOI: 10.1007/s00340-007-2927-9

[24] S.Shmavonyan, A.Khanbekyan, A.Gogyan, M.Movsisyan, A.Papoyan, Selective reflection of light from Rb2 molecular vapor, *Journal of Molecular Spectroscopy*, **313**(2015), 14–18.

[25] A.Weis, V.A.Sautenkov, T.W. Hänsch, Observation of ground-state Zeeman coherences in the selective reflection from cesium vapor, *Phys. Rev. A*, **45**(1992), 7991–7996. DOI: 10.1103/PhysRevA.45.7991

[26] V.A.Sautenkov, H.Li, M.A.Gubin, Y.V.Rostovtsev, M.O.Scully, Variable spectral filter based on optically saturated selective reflection, *Laser Physics*, **21**(2011), 153–157.

[27] A.V.Belinsky, M.K.Shulman, Quantum nature of a nonlinear beam splitter, *Phys. Usp.*, **184**(2014), 1022–1034. DOI: 10.3367/ufnr.0184.201410i.1135

[28] A.Badalyan, V.Chaltykyan, G.Grigoryan, A.Papoyan, S.Shmavonyan, M.Movsessian, Selective reflection by atomic vapor: experiments and self-consistent theory, *The European Physical Journal D*, **37**(2005), 157–162. DOI: 10.1140/epjd/e2005-00258-6

[29] B.Crosignani, P.D.Porto, A.Yariv, Nonparaxial equation for linear and nonlinear optical propagation, *Opt. Lett.*, **22**(1997), 778–780.

[30] V.G.Arkhipkin, S.A.Myslivets, One- and two-dimensional Raman-induced diffraction gratings in atomic media, *Phys. Rev. A*, **98**(2018), 013 838. DOI: 10.1103/PhysRevA.98.013838

[31] R.W.Boyd, Nonlinear optics, London: Academic Press, 1992.

[32] L.Zhao, W.Duan, S.F.Yelin, All-optical beam control with high speed using image-induced blazed gratings in coherent media, *Phys. Rev. A*, **82**(2010), 013 809. DOI: 10.1103/PhysRevA.82.013809

[33] K.Iizuka, Engineering Optics, Vol. 35 of Springer Series in Optical Sciences, 3 edn, Springer–Verlag, New York, 2008.

Эффект Тальбота при селективном отражении от рамановски индуцированной решетки

Василий Г. Архипкин
Сергей А. Мысливец
Институт физики им. Л. В. Киренского СО РАН
Федеральный исследовательский центр КНЦ СО РАН
Красноярск, Российская Федерация
Сибирский федеральный университет
Красноярск, Российская Федерация

Аннотация. В работе исследуется эффект Тальбота при селективном отражении пробного излучения на границе раздела диэлектрик — слой резонансных атомов, в котором индуцируется рамановская решетка. В таких условиях интерфейс может выступать как отражательная дифракционная решетка. Рассмотрены случаи одномерных и двумерных решеток. Показано, что коэффициент отражения с учетом селективно отраженной волны может быть как больше, так и меньше обычного коэффициента отражения Френеля. Эффект Тальбота можно наблюдать для селективно отраженной волны в ближней дифракционной области. Пространственная структура дифракционных картин существенно зависит от напряженности поля накачки и рамановской отстройки.

Ключевые слова: рамановское усиление, дифракция Френеля, эффект Тальбота, селективное отражение.